

We are IntechOpen, the world's leading publisher of Open Access books Built by scientists, for scientists

6,900

Open access books available

186,000

International authors and editors

200M

Downloads

Our authors are among the

154

Countries delivered to

TOP 1%

most cited scientists

12.2%

Contributors from top 500 universities



WEB OF SCIENCE™

Selection of our books indexed in the Book Citation Index
in Web of Science™ Core Collection (BKCI)

Interested in publishing with us?
Contact book.department@intechopen.com

Numbers displayed above are based on latest data collected.
For more information visit www.intechopen.com



Optically Accelerated Formation of One- and Two-Dimensional Holographic Surface Relief Gratings on DR1/PMMA

Xiao Wu, Thi Thanh Ngan Nguyen,
Isabelle Ledoux-Rak, Chi Thanh Nguyen and
Ngoc Diep Lai

Additional information is available at the end of the chapter

<http://dx.doi.org/10.5772/53788>

1. Introduction

Polymer-based periodic structures nowadays are very useful for many applications in optoelectronics and photonics, such as optical filters, distributed-feedback laser, waveguide coupling, photonic crystals, etc. [1-3]. Different methods based on photoinduced transformation of photosensitive materials have been used to fabricate the desired periodic structures. A common point of these fabrication technologies is the use of a so-called photoresist to record the light pattern following by a development process. The later one allows to wash out the remaining unpolymerized photoresists, resulting in a polymerized structure, which is a duplication of the light pattern. However, development techniques based on solvent dissolutions affect the fabrication process, leading often to a deformation of the fabricated structures. Recently, new organic materials named azobenzene-containing polymers (azopolymers) have attracted much attention for the fabrication of sub-micrometer structures, thanks to a particular mass transport effect under a modulated light irradiation. This phenomenon allows to fabricate a so-called surface relief grating (SRG) by a simple one-step process, without development process [4-5]. Figure 1 shows the chemical structure of one typical commercial azopolymer named Disperse Red 1-poly-methyl-methacrylate (DR1/PMMA). Here, the DR1 molecule is attached to the polymer backbone MMA monomers through covalent bonds with a 30/70 molar ratio between them. This copolymer presents very good thermal and temporal stability with high glass transition temperature ($T_g = 125^\circ\text{C}$). Experimental results have been shown that the SRG formation

on an azopolymer film depends on different parameters: sample temperature, light polarization, intensity of the interference beams, etc. Many theoretical models have been proposed to explain the mechanism of SRG formation [6-10] on DR1/PMMA azopolymer. Despite these efforts, the mechanism is still not fully explained. The most plausible and widely used model is the gradient force model [7]. According to this model, the pressure and resultant force can be achieved thanks to the light irradiation, which induces a *trans*-form \leftrightarrow *cis*-form photoisomerization effect in azobenzene molecules. Inset of the Fig. 1 illustrates the photoisomerization process between the *trans*-form and *cis*-form of a DR1 chromophore molecule. At room temperature, the *trans*-form is fundamentally stable as compared with the *cis*-form. When the DR1 molecule is subjected to a visible illumination, the *trans*-form will be transformed to a *cis*-form, which later relaxes back to the *trans*-form by thermal relaxation (slow process) or by UV irradiation (fast process). Under a spatially modulated irradiation, the DR1 molecules, after many *trans*-form \leftrightarrow *cis*-form cycles, will move from the position of highest intensity to the position at which the light intensity is lowest. Therefore, the necessary condition to form the SRG is a photoisomerization process under the irradiation of a modulated light intensity.

This chapter presents the fabrication of one- and two-dimensional (1D and 2D) holographic SRGs based on one- or multi-exposure of the azobenzene copolymer (DR1/PMMA) to two- and/or three-beam interference patterns. A single exposure of the two-beam interference pattern is used to form 1D SRG. 2D periodic structure then can be fabricated either by two exposures of the sample to a two-beam interference pattern or by only a single exposure to a three-beam interference pattern. Also, the formation of SRGs is optically accelerated by assisting it with an independent UV or VIS laser.

Section 2 shows the fabrication of SRG by using the two-beam interference technique. Because of the important role of the intensity and polarization modulations during the formation of SRG, the theory of two-beam interference will be presented in detail. The diffraction efficiency (DE) and the depth of SRGs fabricated with different polarization configurations have been characterized and discussed. The relationship between the depth and period of SRG was also studied and reported. The 2D holographic SRG is realized by using two exposures to the two-beam interference pattern. This fabrication method is simple and easy to control the SRG periodicity, but it is time consuming and the 2D SRG structures are not symmetric.

In order to rapidly fabricate uniform and symmetric 2D SRG structures, the three-beam interference technique has been used as shown in Section 3. The theory of three-beam interference is first studied, analysing in particular the influence of polarizations of the three laser beams on the intensity and polarization modulations. Then, 2D hexagonal structures have been fabricated by this fabrication technique with a particular polarization configuration (circular-circular-circular). Comparison with the results obtained by the multiple-exposure two-beam interference technique and discussions of the advantages of this technique will also be presented.

In Section 4, we investigate experimentally the optimization of 1D SRG formation by using an additional laser to assist the photoisomerization process. First, an UV beam (355 nm-wave-length) is used to accelerate the photoisomerization from the *cis*-form to the *trans*-form. Second,

a VIS beam (532 nm-wavelength), of the same wavelength as the interference beams, is used to accelerate the photoisomerization from the *trans*-form to the *cis*-form. Both techniques allowed to enhance the SRG formation, resulted in a better DE and a larger depth of the SRGs. The mechanisms of these two methods are different but both of them are polarization dependent.

Finally, we will make some conclusions of our work and also release some prospects.

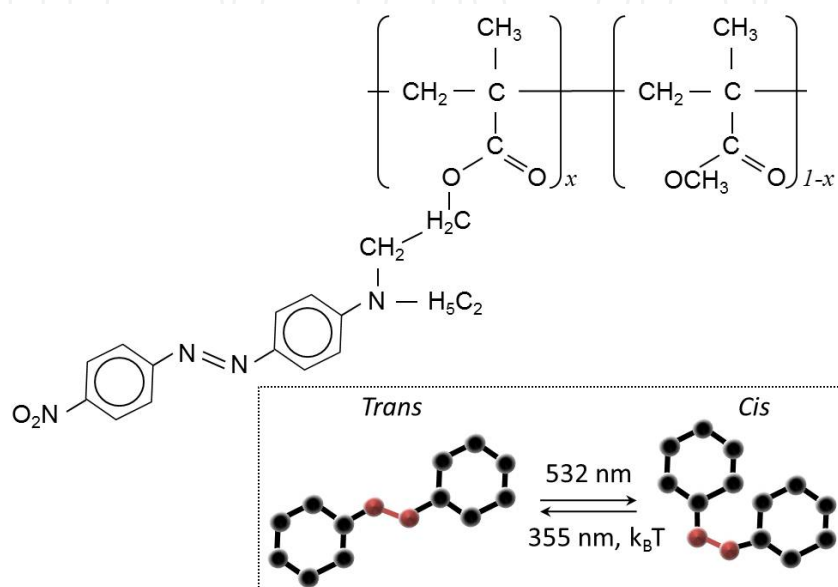


Figure 1. Chemical structure of the DR1/PMMA copolymer. Insert shows the *trans*-form \rightarrow *cis*-form photoisomerization process induced by different optical excitations and thermal relaxation.

2. Two-beam interference

Laser interference technologies have been widely used to fabricate polymer-based periodic and quasi-periodic micro- and nano-structures with large areas. We propose to use the two-beam interference technique to fabricate 1D and 2D SRG structures by one- and two-exposure. Indeed, two-beam interference is the simplest configuration (Fig. 2(a)), which allows to create a spatial modulation of light intensity in one dimension.

2.1. Theory of two-beam interference

Considering two-beam interference as illustrated in Fig. 2(a). Two coherent laser beams of the same profiles and same intensities and coming from the same laser source propagate toward the same sample area. These laser beams are symmetrically oriented around the sample normal direction and make an angle θ with respect to this axis. The electric fields, $E_1(\mathbf{r}, t)$ and $E_2(\mathbf{r}, t)$, of the two plane waves corresponding to these two laser beams are given by

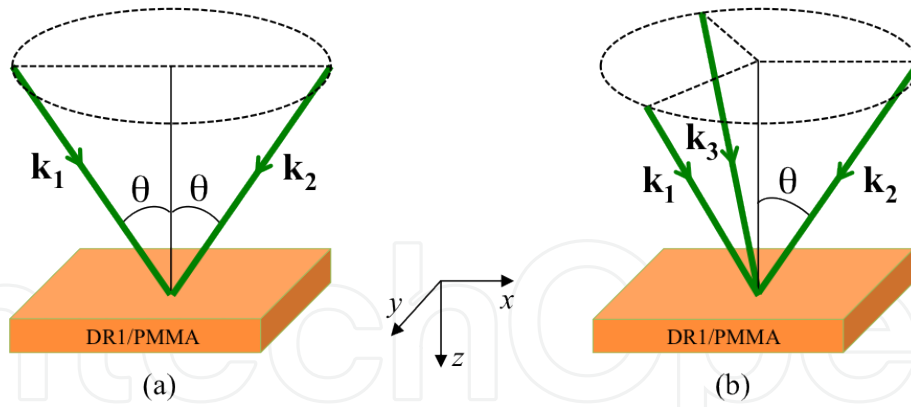


Figure 2. Optical arrangement of two-beam (a) and three-beam interference (b) techniques. Each laser beam is symmetrically oriented around the vertical axis by an angle θ . \mathbf{k}_i ($i = 1, 2, 3$) represents the wave vector of each laser beam.

$$\mathbf{E}_1(\mathbf{r}, t) = \text{Re} \left[E_{01} \exp(i(\mathbf{k}_1 \cdot \mathbf{r} - \omega t)) \mathbf{e}_1 \right], \tag{1}$$

$$\mathbf{E}_2(\mathbf{r}, t) = \text{Re} \left[E_{02} \exp(i(\mathbf{k}_2 \cdot \mathbf{r} - \omega t)) \mathbf{e}_2 \right], \tag{2}$$

where \mathbf{k}_1 and \mathbf{k}_2 are the corresponding wave vectors, \mathbf{r} is the position vector in the overlapping space, E_{01} and E_{02} are the real electric field amplitudes, and \mathbf{e}_1 and \mathbf{e}_2 are the unit vectors of the polarizations. At the overlapping area of the two beams, the interference electric field is the sum of the electric fields of individual plane waves

$$\mathbf{E}_T(\mathbf{r}, t) = \mathbf{E}_1(\mathbf{r}, t) + \mathbf{E}_2(\mathbf{r}, t). \tag{3}$$

The interference intensity distribution of the resultant wave is given by

$$I_T(\mathbf{r}, t) = \langle \mathbf{E}_T^*(\mathbf{r}, t) \cdot \mathbf{E}_T(\mathbf{r}, t) \rangle_t, \tag{4}$$

where $\langle \dots \rangle_t$ represents the time average of the resultant electric field.

Using equations (3) and (4), we can easily calculate both the intensity distribution and the polarization distribution of the interference pattern. The periodicity of the interference pattern depends on the angle θ and the laser wavelength (λ), and it is determined by

$$\Lambda = \frac{\lambda}{2 \sin \theta}. \tag{5}$$

In this work, all numerical calculations were realized by using Matlab software with personal codes, which allowed to investigate all properties of the interference pattern as a function of different polarizations of the laser beams.

2.1.1. Intensity distribution

Figure 3 shows the simulation results of the intensity modulation of the two-beam interference pattern, obtained with different polarization configurations and at different incident angles θ . We have considered four particular polarization configurations of the two laser beams: S-S, P-P, S-P, and RC-LC (right circular and left circular). Since the interference cannot be realized with S-P polarization configuration, this particular case is not shown here. For the three other polarization configurations, we can see that intensity modulation depends not only on the polarization configuration, but also on the incident angle θ . Namely, for a S-S polarization configuration, the polarizations are the same for both laser beams at any angle θ , resulting in a maximal amplitude modulation (100%) of the intensity interference pattern. However, the amplitude modulation increases from 0 to 100% when θ increases in the case of RC-LC polarization configuration. Also, for the P-P configuration, the amplitude modulation firstly decreases then increases when θ varies from 0° to 90° . We note that for the last case, there is a position shifting the interference pattern by a distance of $\Lambda/2$ along x -axis for $\theta = 45^\circ$, but this does not affect the fabrication of SRGs.

In order to evaluate the influence of polarizations configurations on the intensity modulation, we introduce a well-known parameter called visibility (interference contrast), C

$$C = \left| \frac{I_T^{\max} - I_T^{\min}}{I_T^{\max} + I_T^{\min}} \right|, \quad (6)$$

where I_T^{\max} and I_T^{\min} are the maximum and minimum of the intensity, respectively.

Figure 4 shows the interference contrast as a function of θ (from 0° to 85°) for different polarization configurations. It is clear that the interference contrast is constant for S-S polarization configuration and keeps increasing with θ for the RC-LC polarization configuration. On the other hand, for the P-P case, the interference contrast decreases from 100% to 0 when the incident angle is varied from 0° to 45° , then increases again from 0 to 100% when θ increases from 45° to 90° . The reason is that in the case of P-P polarization configuration, two polarizations tend to be orthogonal when θ approaches 45° . At this particular angle, two polarizations are perpendicular and there is no interference. Therefore, for a standard optical lithography, a two-beam interference pattern with S-S polarization configuration is used in order to ensure the best intensity modulation contrast.

2.1.2. Polarization modulation

However, when the two-beam interference technique is applied to SRG formation, the modulation condition of the interference intensity is not enough, since the photoisomerization of DR1 molecules depends also on the illuminated light polarization. The polarization

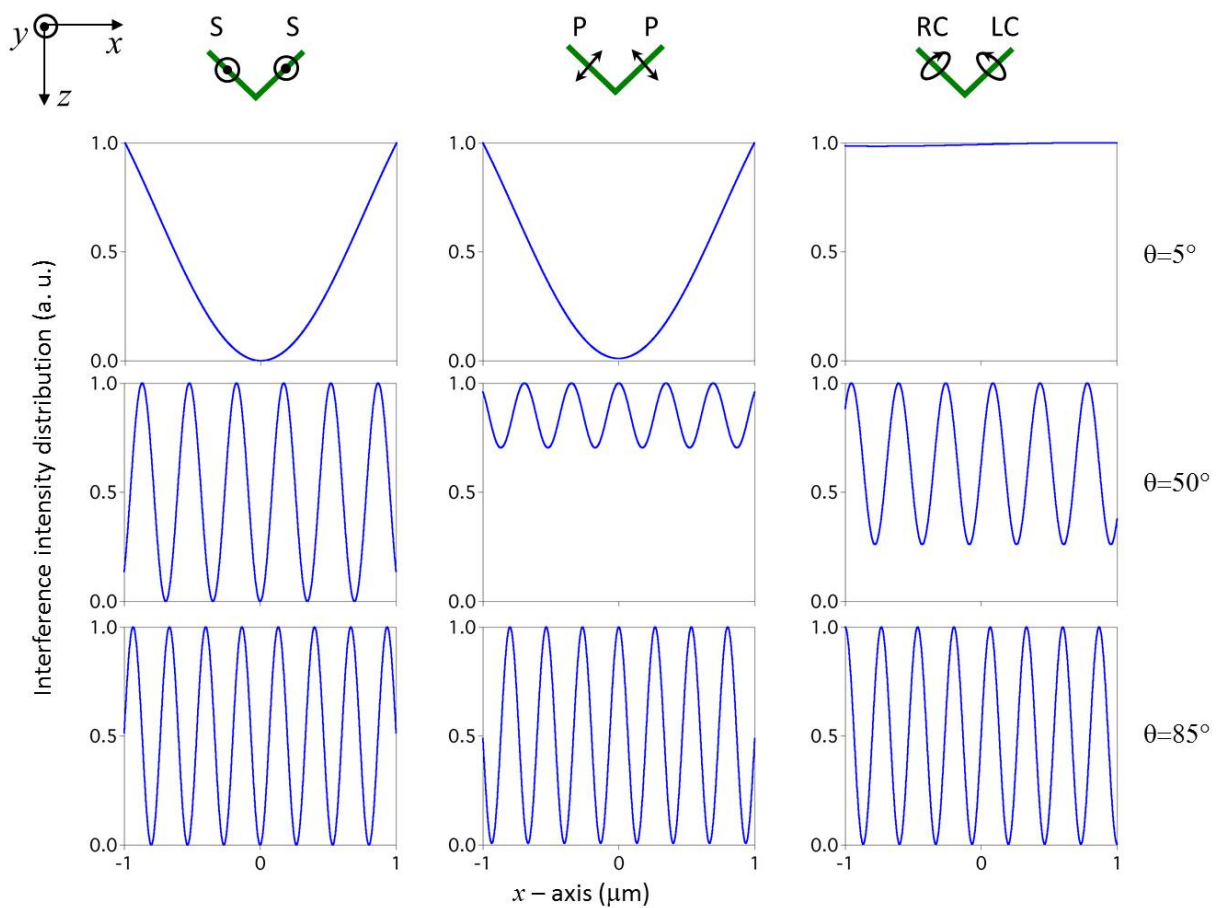


Figure 3. Interference intensity distributions along the x -axis, calculated for different polarizations configurations (S-S, P-P, RC-LC) at $\theta = 5^\circ$, 50° and 85° , respectively. S and P represent two orthogonal linear polarizations; RC and LC are right and left circular polarizations, respectively. Note that: i) the intensity modulation keeps the same shape (except periodicity) for any θ -value in the case of S-S polarization configuration; ii) there is a $\lambda/2$ switching position of the interference pattern for $\theta = 45^\circ$ in the case of P-P polarization configuration, and iii) there is no intensity modulation at any θ -value in the case of S-P polarization configuration (not shown).

distribution of the resultant field of the two laser beams has been then evaluated. Figure 5 represents the polarization distributions of the two-beam interference pattern in the xy -plane for different polarization configurations and for different incident angles. The background illustrates the intensity pattern where the deep colour corresponds to high intensity and the light colour corresponds to low intensity. The polarization of the resultant field is calculated for several particular positions, corresponding to $x = \pm\lambda/2$; $\pm\lambda/4$; 0. For the S-S polarization configuration, the interference polarization keeps the same direction, as those of the two laser beams, for any position and for all incident angles. In the case of the P-P polarization configuration, the interference polarization direction is also the same for different θ -values, but the polarization amplitude decreases with increasing θ . In fact, when θ increases, the polarizations of both laser beams become parallel to the z -axis, i. e. perpendicular to the xy -plane, resulting in a diminution of the interference polarization amplitude in this plane. For the two other polarization configurations, the interference polarization varies periodically between linear,

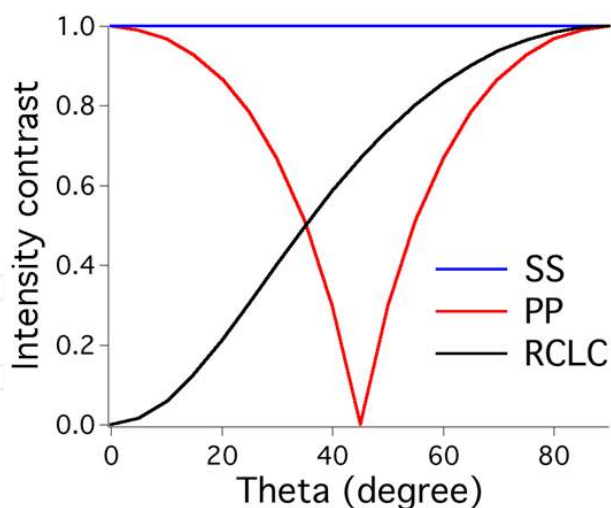


Figure 4. Interference contrast or visibility of the two-beam interference pattern as a function of the angle θ . Three curves are obtained by using different polarizations configurations (S-S: blue line, P-P: red line, RC-LC: black line). There is a $\Lambda/2$ switching position of the interference pattern for $\theta = 45^\circ$ in the case of P-P polarization configuration, corresponding to a minimum contrast at this angle.

elliptic and circular forms, as seen in Fig. 5. In particular, for the S-P polarization configuration, a periodical modulation of the resultant polarization is obtained, while the resultant intensity modulation cannot be achieved, as discussed above. That will explain why SRG can be realized with such polarization configuration, thanks to the interference polarization modulation. Finally, for the case of RC-LC polarization configuration, the resultant polarization becomes a linear polarization for any θ -value, but the polarization direction changes periodically in the xy -plane. We note that, similar to the case of P-P polarization configuration, the polarization amplitude in the xy -plane decreases when θ increases. Besides, the interference polarization pattern is shifted by a distance of $\Lambda/4$ along the x -axis with respect to the interference intensity pattern, as shown in Fig. 5.

As discussed before, the formation of SRG on azo-copolymer depends on the modulation of the irradiating light pattern and also on its resultant polarization. Therefore, polarization modulation and intensity distribution of the interference pattern are two necessary conditions, complementary and also competitive, for creating SRG. In this work, different SRGs were experimentally realized and the polarization dependence in the formation of SRG was also investigated.

2.2. Experimental demonstration

SRGs were fabricated by the following procedure: i) preparation of a thin film sample by spin-coating DR1/PMMA on cleaned glass substrate and baking in the oven at a temperature of 120°C for 2 hours to remove the solvent; ii) exposure by a two-beam interference pattern.

In order to build-up the fabrication technique, we have first recorded the UV-Visible absorption spectrum of the DR1/PMMA thin film. The absorption band ranges from 400 nm to 570

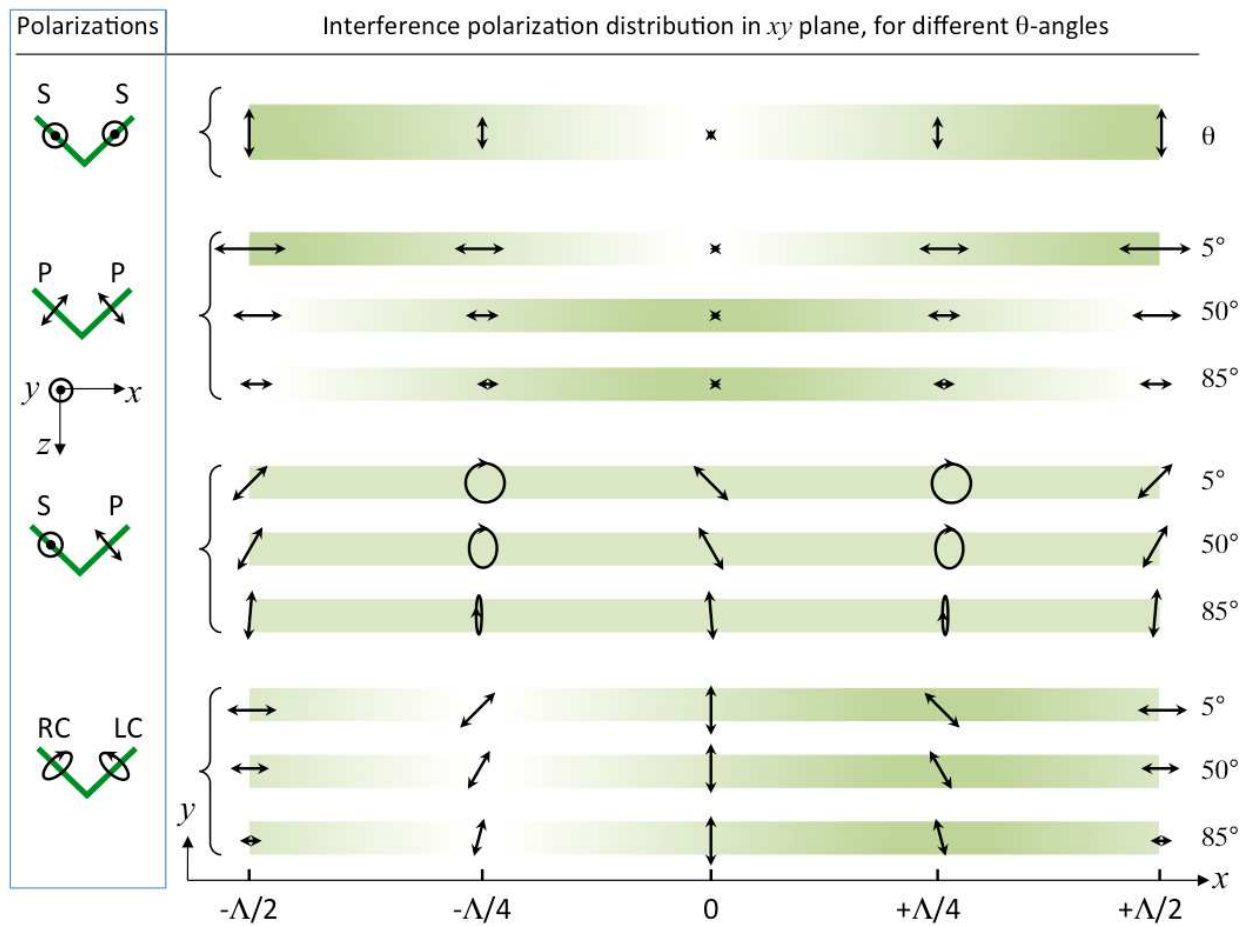


Figure 5. Polarization distributions in xy -plane of the two-beam interference pattern, obtained with different polarization configurations. The interference pattern is calculated for one period (from $-\Lambda/2$ to $+\Lambda/2$). The polarization modulation varies as a function of θ -values (5° , 50° and 85°). The white-green colour of the background represents intensity interference pattern.

nm, with an absorption peak at 480 nm. A green laser is therefore suitable for the SRG formation.

The experimental setup for two-beam interference can be realized easily according to Fig. 2 (a). A green laser ($\lambda = 532$ nm) beam is split into two identical secondary beams by a 50/50 non-polarized beam splitter. The two beams were then combined, by using two mirrors, and interfered on the azo-copolymer film. The polarizations of the two laser beams were controlled independently by using different wave plates (quarter-wave plate and half-wave plate). The incident angle θ was adjusted by tuning the two mirrors symmetrically, and the SRG periodicity varied from several micrometers to hundreds nanometers. The intensity of each interference beam was fixed to about 84 mW/cm^2 at the sample position. In order to monitor the dynamics of SRG formation, a red laser beam ($\lambda = 633$ nm, power = 1 mW) was sent into the interference area, and the first-order diffraction intensity was measured as a function of time, indicating the formation of SRG. The fabricated SRGs were then examined by using an atomic force microscope (AFM) and/or a scanning electron microscope (SEM).

2.2.1. Formation of SRG with different polarization configurations

Figure 6 shows experimental results of the SRGs formation. The incident angle θ is 9° , corresponding to a grating period of $1.7 \mu\text{m}$. Figure 6(b) shows the AFM image of a 1D SRG obtained by the RC-LC polarization configuration, which is perfectly consistent with the simulation result of the interference pattern illustrated in Fig. 6(a). Actually, the shape of the interference intensity pattern and that of SRG are similar, with a sinusoidal form of the same period. However, we note that the highest intensity of the interference pattern corresponds to the valley of SRG, due to the mass transport effect, which induces the transfer of the DR1 molecule from high intensity to low intensity area.

Figures 6(c) and (d) show the first-order diffraction efficiency (DE) and the amplitude of the SRGs fabricated using different polarization configurations. Note that the probing beam (red laser) applied to the film surface during the whole formation process has no influence on the sample structure because its wavelength is out of the absorption band of the DR1 molecules [11]. Figure 6(c) shows the time dependence of the DE, which is obviously polarization dependence. The diffraction signal indicates the creation of the SRG and depends on the exposure time. For all the polarization configurations, DE increases as a function of time, except for the RC-LC polarization configuration for which DE saturates and decreases after 10 min of exposure. However, we note that during the light irradiation process, the DE results from the formation of three different gratings for the azobenzene copolymer: two gratings were caused by refractive index change in the bulk copolymer material because of the different refractive index values between *trans*-form and *cis*-form of DR1, and only the third one is related to SRG [12]. An investigation of the SRG amplitude is necessary to fully analyse the polarization dependence of the SRG formation.

Figure 6(d) shows the amplitude of the SRGs measured by AFM. The time-dependence of the SRG depth is similar to that of the first-order diffraction intensity, except in the case of RC-LC polarization configuration, for which SRG depth doesn't decrease after saturation. This explains the behaviour observed in Fig. 6(c) for RC-LC polarization configuration, in which there is an exchange of the DE between the three different gratings, i. e. while the DE of two other refractive gratings increases then decreases, the DE of the SRG just continues to increase. We conclude that the SRG formation plays a dominant role in DE evolution.

Besides, we also found that the RC-LC polarization configuration is the best case, which allows to achieve SRGs with the largest amplitude, as seen in Fig. 6 (d). On the other hand, the S-S polarization configuration, theoretically providing 100% of intensity modulation, allows obtaining SRGs with a depth of only several tens nanometers. Surprisingly, even in the case of S-P polarization configuration, which does not create any intensity modulation, allows to obtain SRGs with large depth, similar to those obtained by using a P-P polarization configuration. The formation of SRGs therefore depends strongly on the polarization distribution, or more precisely, it depends on the compromise between the intensity and the polarization modulations. Furthermore, we observed that the SRG depth reaches to a saturation level and remains unchanged after. This saturation level depends mostly on the thickness of the sample, on the light irradiation intensity, and also on the periodicity of the interference pattern. The dependence of the SRG formation with respect to the two first parameters has been studied

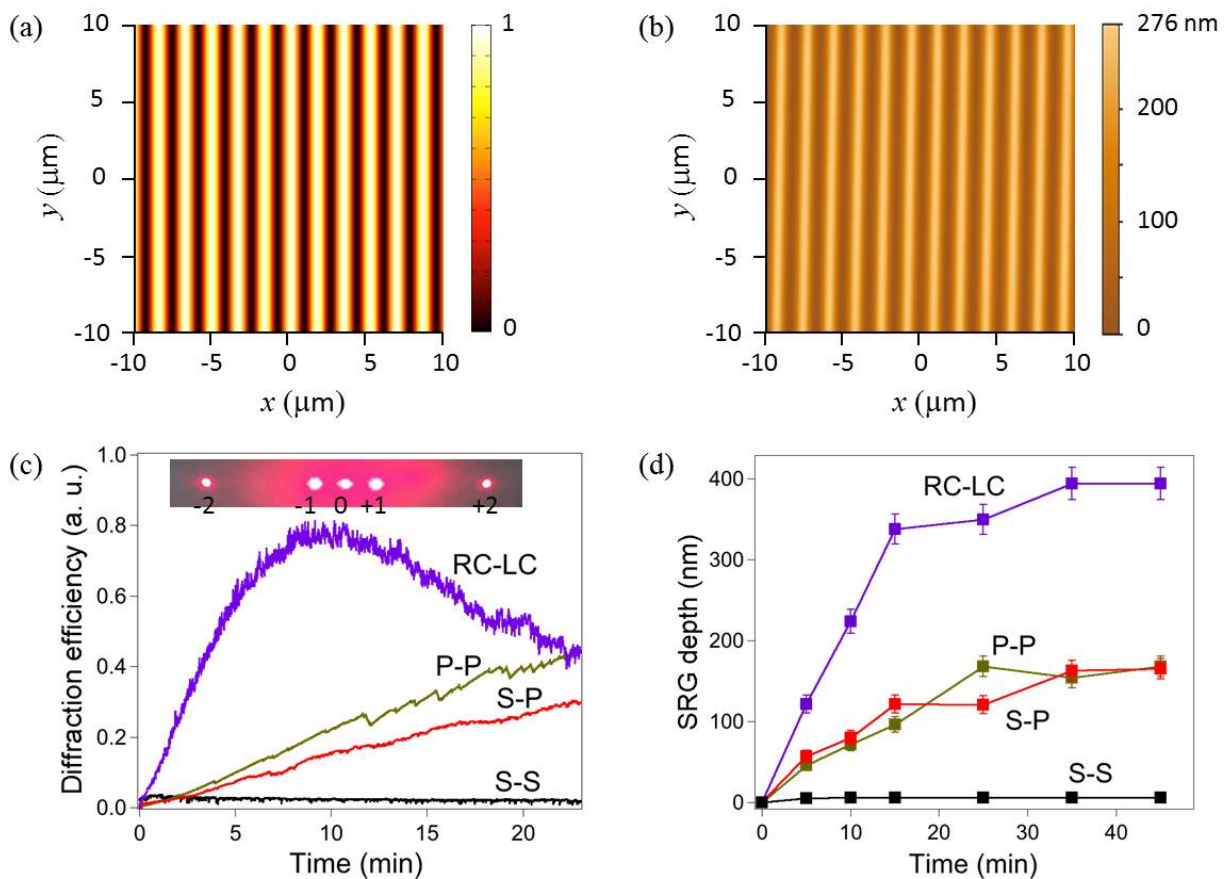


Figure 6. Surface relief grating inscribed on DR1/PMMA by two-beam interference technique. (a) Theoretical calculation of the light intensity distribution of the two-beam interference pattern. (b) AFM image of a fabricated 1D SRG. (c) Time evolution of the first-order diffraction intensity, obtained by sending a red laser beam at a normal incidence to the 1D SRG. Insert shows the experimental diffraction pattern. (d) SRG depths measured as a function of exposure time for different polarization configurations.

before [13, 14], and those parameters are kept unchanged in our case. In the next section, we will show the influence of the periodicity of the interference pattern on the SRGs depth, in order to find out the best SRG, i.e. the smallest period with large amplitude, for our applications in nanophotonic domain.

2.2.2. SRG depth versus interference periodicity

The periodicity of the two-beam interference was varied and all other parameters were kept the same for this investigation. The thickness of the azo-copolymer film is about 1.7 μm. The exposure time is fixed at 40 min, which is long enough to achieve the saturation of the grating formation. The polarizations of the two laser beams are RC-LC configuration to ensure the best SRGs amplitude. According to equation (5), the SRG period can be adjusted with the incident angle θ to a minimal value of $\lambda/2$, equivalent to approximately 270 nm. Figure 7 shows the experimental results of the relationship between the SRG period and depth.

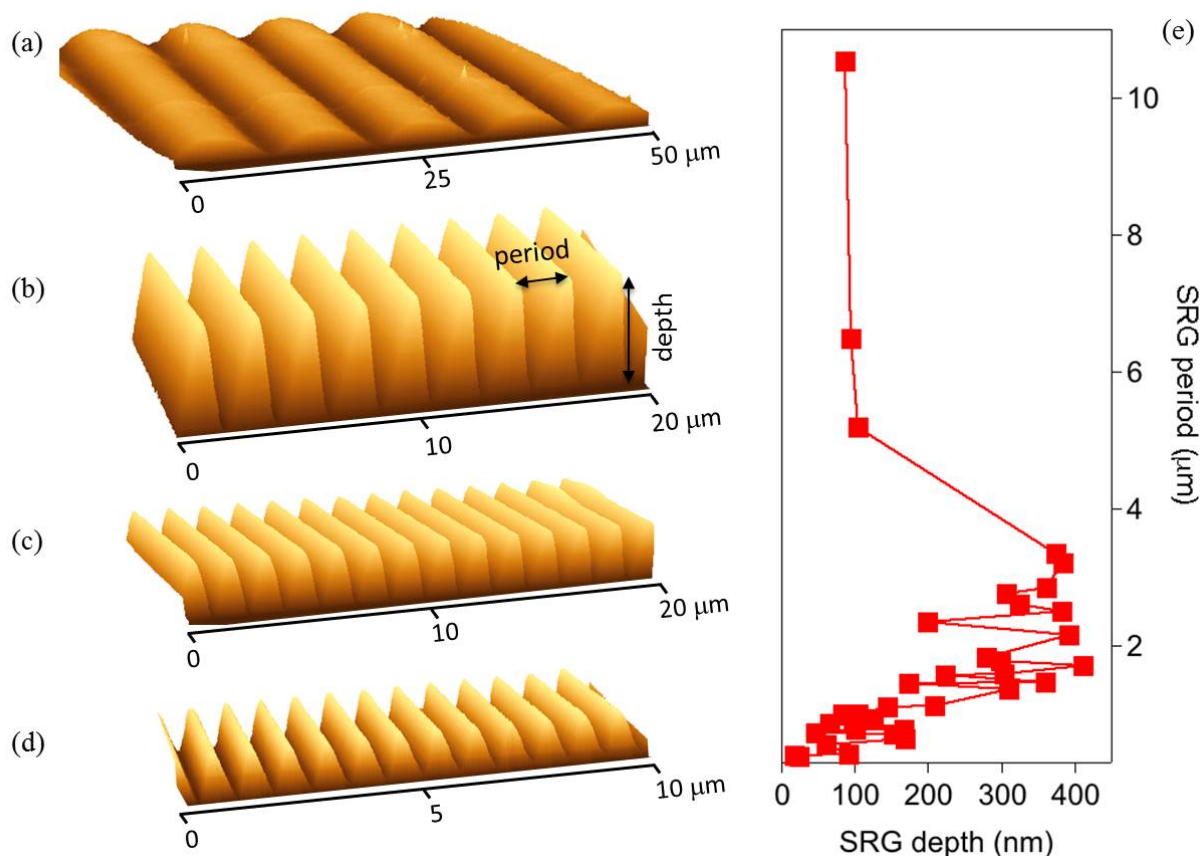


Figure 7. The dependence of SRG depth on the interference periodicity. (a-d) AFM images of SRG structures obtained with different θ -values. (e) SRG depth as a function of the SRG period.

Figures 7(a-d) show the AFM images of several examples of 1D SRGs with different periods ((a): 10 μm , (b): 2 μm , (c): 1.5 μm , and (d): 0.7 μm). As expected from the intensity modulation (Fig. 4) and polarization modulation (Fig. 5), the SRG amplitude is not constant, but varies as a function of the θ -value. Figure 7(e) shows how the SRG amplitude depends on the grating period. The best SRG with the largest amplitude, of about 400 nm, was obtained with Λ between 1.5 μm and 3 μm . The SRG amplitude decreases outside of this period range ($>3 \mu\text{m}$ or $<1.5 \mu\text{m}$), but SRG can be still created with Λ values as large as 10 μm , or as small as 0.38 μm . In literature [15-16], people tried to explain this phenomenon including of a compromise of the intensity and the polarization modulation. However, it is quite difficult to explain the dependence of SRG depth on its period. Various elements should be considered to explain this dependence. For example, Kim et al. [15] suggested that the thermal effects resulting from absorption of light contribute to this phenomenon. But it cannot explain the sharp drop of the depth for smaller periods ($<0.8 \mu\text{m}$). Barret et al. [17] have used the photoisomerization pressure model to explain the mass transport effect, which led to a relationship between the SRG period and depth. However, their theoretical prediction and the experimental observations do not match well.

In our point of view, the dependence of the SRG depth on period should be explained by taking into account the effective movement distance of the azo-copolymer material under light irradiation. Actually, light induces the photoisomerization effect and pushes the azo-copolymer material away from high exposure intensity to dark areas over an effective distance of several hundred nanometers [18]. For a large period, this movement distance is too short to match with Λ , and cannot help to create a SRG with large amplitude. When the SRG period is smaller than the movement distance, the azo-copolymer will move from highest intensity to lowest intensity areas, and even to the next highest intensity area. A mixing movement in different areas happens and the barrier between lowest and highest intensity is not clearly identified, leading to a decrease of the SRG amplitude. Finally, there exists a range of periods, in which the movement distance of the azo-copolymer is matched with the distance between highest and lowest intensities of the interference pattern, leading to a best formation of the SRG with largest amplitude. These arguments are well consistent with our experimental observations. We note also that the movement distance of the azo-copolymer, accordingly the optimum SRG period and depth, depends strongly on different experimental parameters, such as the sample thickness, the light wavelength and intensity, the temperature, etc.

2.2.3. Formation of 2D SRG by two exposures

Recently, the multi-exposure of two-beam interference technique has been demonstrated to be very powerful to fabricate desired 2D and 3D structures on photoresists [19-20]. Here, the same method was used to realize 2D structures on DR1/PMMA. In practices, after the first exposure, the sample was rotated by an α -angle around the z -axis, and then was exposed for a second time to the same interference pattern.

Figure 8 shows the simulation and the corresponding experimental results by setting the rotational angle of 90° or 60° between two exposures to the two-beam interference pattern. As can be seen in Fig. 8 (a, b), we predicted a fabrication of a square or hexagonal structure with symmetric form. Figures 8 (c, d) show that 2D square and hexagonal structures were effectively fabricated on the DR1/PMMA. The corresponding diffraction patterns shown in Fig. 8 (e, f) also explain the periodicities of fabricated 2D structures. However, as can be seen in Fig. 8(c-f), the 2D structures fabricated in DR1/PMMA, by using two exposures of two-beam interference technique, are not symmetric with respect to the two directions of fabrication, as indicated by the 1 and 2 axis. AFM results also show that the SRG depths are different in these two directions. It is clear that the mechanism of the SRG formation is different from that of the fabrication of 2D structures on photoresists. Indeed, after the first inscription, a 1D SRG was created and the thickness of DR1/PMMA in the regions of peaks was increased with respect to the thickness of original film. The second exposure therefore dealt with a non-uniform film, which makes the fabrication of a final symmetric 2D structure difficult. In order to obtain such a 2D symmetric SRG, the exposure time of the second exposure should be much longer than that of the first exposure. The control of the exposure dose ratio between two exposures has been considered [21], but this method lacks of reproducibility. Indeed, the SRG formation depends on many experimental parameters and the SRG depth does not reach the same value for different samples or different fabrication times.

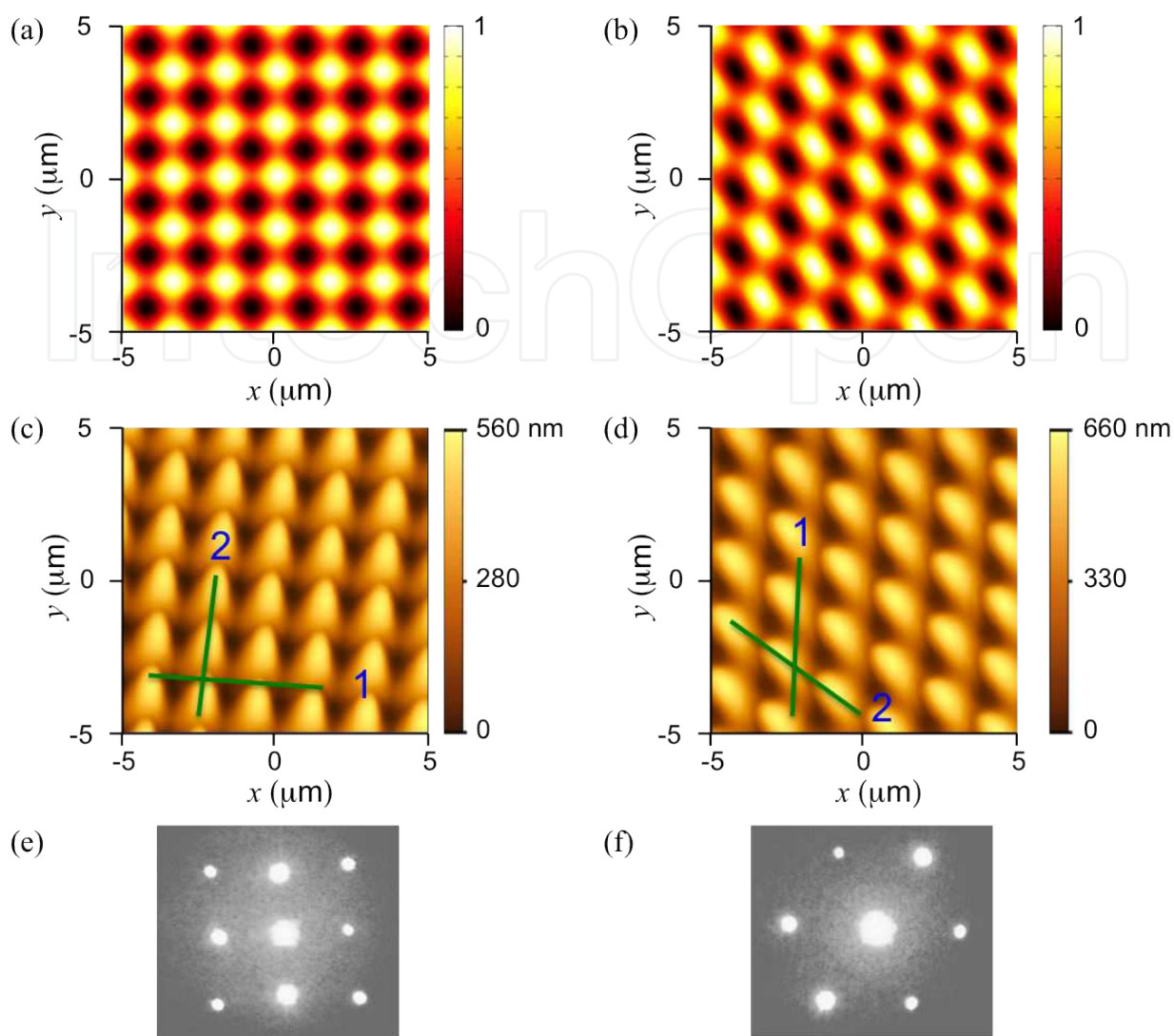


Figure 8. Square and hexagonal SRG structures fabricated by two exposures of two-beam interference pattern with a rotation angle of 90° and 60° between the two exposures, respectively. (a), (b) Theoretical calculation of light intensity distribution, and (c), (d) corresponding experimental results, respectively. (e), (f) Diffraction patterns of the square and hexagonal structures, respectively.

Therefore, in order to create 2D symmetric SRGs on an azo-copolymer material, a single exposure of a three-beam interference pattern is necessary. In the next section, we report our investigations on the use of this interference technique.

3. Three-beam interference

Three-beam interference has been successfully employed to fabricate hexagonal periodic structures [22]. In the case of a standard fabrication on photoresist, the information of three-beam interference resultant polarization is often ignored. However, when this method is applied to the formation of SRG, both intensity distribution and polarization distribution of

the interference pattern play important roles. In this section, we present in detail the properties of the three-beam interference technique, using different possible polarization configurations.

3.1. Theory of three-beam interference

Figure 2 (b) shows the beams geometry of the considered three-beam interference. The three laser beams are symmetrically aligned around the z-axis with the same incident angle θ . Similar to the case of two-beam interference, the three beams are associated to three plane waves $E_1(\mathbf{r}, t)$, $E_2(\mathbf{r}, t)$ and $E_3(\mathbf{r}, t)$, whose electric fields are given by

$$E_1(\mathbf{r}, t) = \text{Re} \left[E_{01} \exp(i(\mathbf{k}_1 \cdot \mathbf{r} - \omega t)) \mathbf{e}_1 \right], \quad (7)$$

$$E_2(\mathbf{r}, t) = \text{Re} \left[E_{02} \exp(i(\mathbf{k}_2 \cdot \mathbf{r} - \omega t)) \mathbf{e}_2 \right], \quad (8)$$

$$E_3(\mathbf{r}, t) = \text{Re} \left[E_{03} \exp(i(\mathbf{k}_3 \cdot \mathbf{r} - \omega t)) \mathbf{e}_3 \right], \quad (9)$$

where \mathbf{k}_1 , \mathbf{k}_2 and \mathbf{k}_3 are the corresponding wave vectors, \mathbf{r} is the position vector in the overlapping space, E_{01} , E_{02} and E_{03} are the real electric field amplitudes, and \mathbf{e}_1 , \mathbf{e}_2 and \mathbf{e}_3 are the unit vectors of the polarizations. In our simulations, we assumed that $|\mathbf{k}_1| = |\mathbf{k}_2| = |\mathbf{k}_3| = k$ and $E_{01} = E_{02} = E_{03} = E_0$. At the overlapping area of the three beams, the interference electric field is the sum of the electric fields of individual plane waves, $\mathbf{E}_T(\mathbf{r}, t) = E_1(\mathbf{r}, t) + E_2(\mathbf{r}, t) + E_3(\mathbf{r}, t)$. The interference intensity is calculated by using equation (4). A 2D periodic structure was then generated with a periodicity determined by $\Lambda = \lambda / (1.5 \sin \theta)$, where λ is the wavelength of laser beam.

Similar to the case of two-beam interference, we have investigated the intensity distribution and the polarization distribution of the three-beam interference pattern as a function of the polarizations of the three laser beams. We considered four particular polarizations configurations, namely, three random polarizations (R,R,R), three p-polarizations (P,P,P), three s-polarizations (S,S,S), and three circular polarizations (C,C,C), as shown in the top of Fig. 9.

3.1.1. Intensity distribution

Figure 9 represents the intensity distributions of the three-beam interference pattern with different polarization configurations. All simulated hexagonal structures are symmetric and have the same period, but their forms change for different polarization configurations. For example, we obtained air-hole structures (low intensity spots) with P,P,P or S,S,S polarization configuration, and dielectric-cylinder structures (high intensity spots) with C,C,C polarization configuration. The intensity contrast varies from this case to the other. The bottom line of Fig. 9 shows the intensity distributions along the x -axis of each case. Note that the contrast also

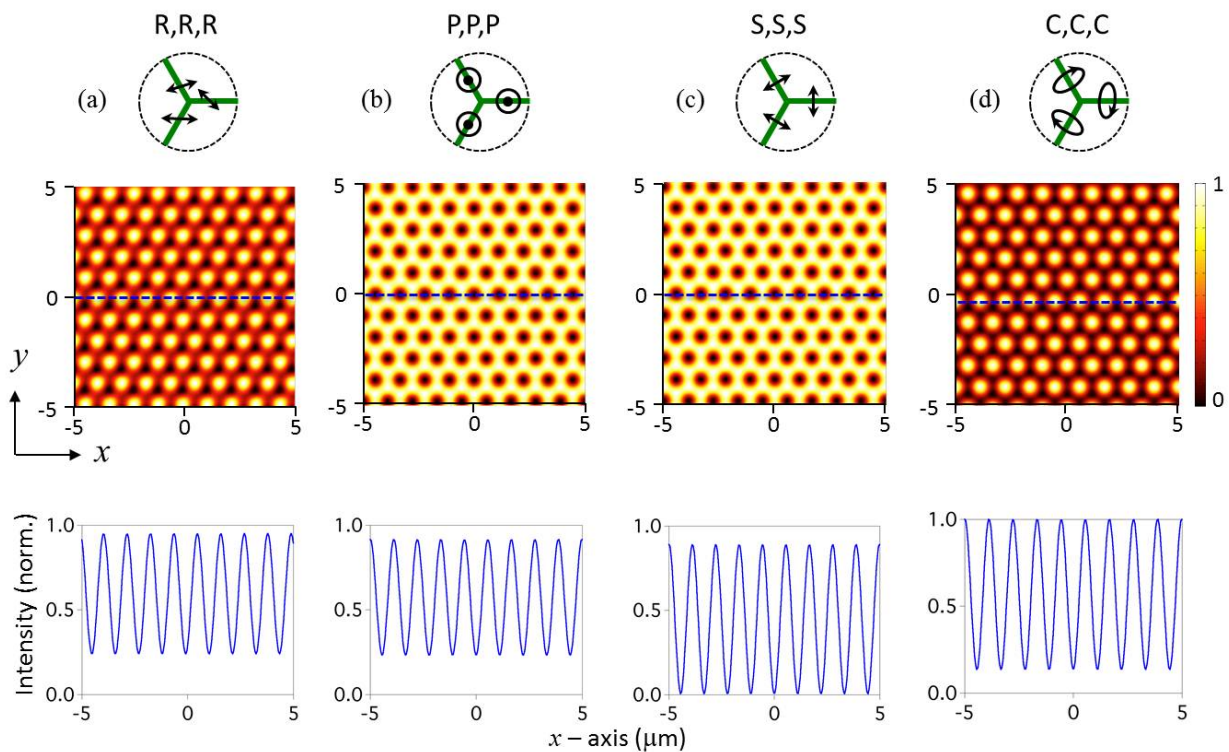


Figure 9. Theoretical calculation of the three-beam interference intensity patterns with different polarization configurations. Polarization arrangements: (a) three random polarization beams; (b) three p-polarization beams; (c) three s-polarization beams; and (d) three circular polarization beams. The interference patterns are all symmetric in xy -plan, but the intensity modulation never reaches 100% for all the cases.

varies as a function of the incident angle θ . However, we show here only results corresponding to the case of $\theta=17.65^\circ$, as it will be realized experimentally and shown in the next section. Theoretically, we expected that this three-beam interference technique allows to create 2D symmetric SRG, by using any polarization configuration.

3.1.2. Polarization modulation

We now consider only three particular polarization configurations, i.e., P,P,P, S,S,S and C,C,C. Because of the periodicity of the interference pattern, it is necessary to calculate the resultant polarization for only one particular area corresponding to a so-called Wigner-Seitz primitive cell. Figure 10 shows thus polarization distributions in the xy -plane for the three cases. We can see that the resultant polarization changes as a function of the considered position. The polarization distributions are also different from this configuration to the other. However, the interfering polarizations are all symmetrically distributed around the origin of Wigner-Seitz primitive cell. Concretely, for P,P,P and S,S,S cases, the resultant polarization is changed from linear to elliptic and to circular. But for the C,C,C case, the resultant polarization keeps the same polarization (circular) throughout the interference pattern. With the SRG samples obtained using the two-beam interference technique, it is difficult to predict the best polarization configuration enabling the fabrication of SRGs with the largest amplitude. However,

from the point of view of fabrication setup, it is quite easy to build-up a three-beam interference technique with C,C,C polarizations, as it will be demonstrated in the next section.

3.1.3. Experimental demonstration

Figure 11 shows the experimental setup of the three-beam interference and the experimental results of 2D hexagonal SRG realized on the DR1/PMMA material. A large and uniform laser beam with circular polarization was split into three sub-beams by a non-polarized multi-surface prism. These three sub-beams, corresponding to three surfaces denoted as A_1 , A_2 , and A_3 , respectively (Fig. 11(a)), show different propagation directions after passing through the prism and then overlap on the surface of the sample. These three beams have the same intensities and same polarizations (circular). This compact system allows to realize a 2D hexagonal structure by only one exposure, which corresponds to the theoretical calculation of the C,C,C polarization configuration shown before. We note that other polarization configurations could be also realized from this setup, but it requires the use of three other mirrors and also different wave plates (quarter-wave and half-wave plates) to control the polarization of each laser beam. In this work, we experimentally demonstrated the fabrication of 2D SRG by using only the simple C,C,C polarization configuration.

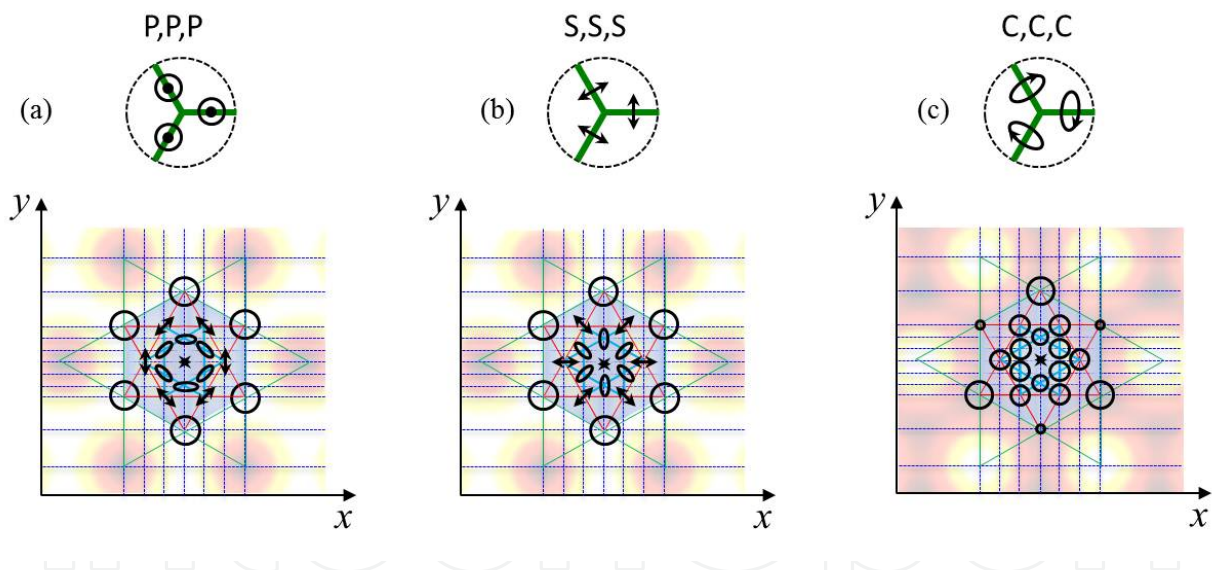


Figure 10. Polarization distributions of the three-beam interference pattern, calculated for one Wigner-Seitz primitive cell. The polarizations vary in different ways for three particular polarization configurations, but all distributions display a 3-fold ~ 6-fold symmetry.

The special design of the tri-prism results in a hexagonal structure with a period of $1.2 \mu\text{m}$ (corresponding to $\theta=17.65^\circ$). With only one exposure of a green laser (532 nm) via the multi-surface-prism, a 2D hexagonal SRG was then created, as shown in Fig. 11(b). The 2D SRG is quite uniform and symmetric. Actually, Fig. 11(c) shows a symmetric diffraction pattern of fabricated structure. The surface modulation along different directions was also characterized, and possessed the same modulation depth, as illustrated in Fig. 11(d). However, we remark

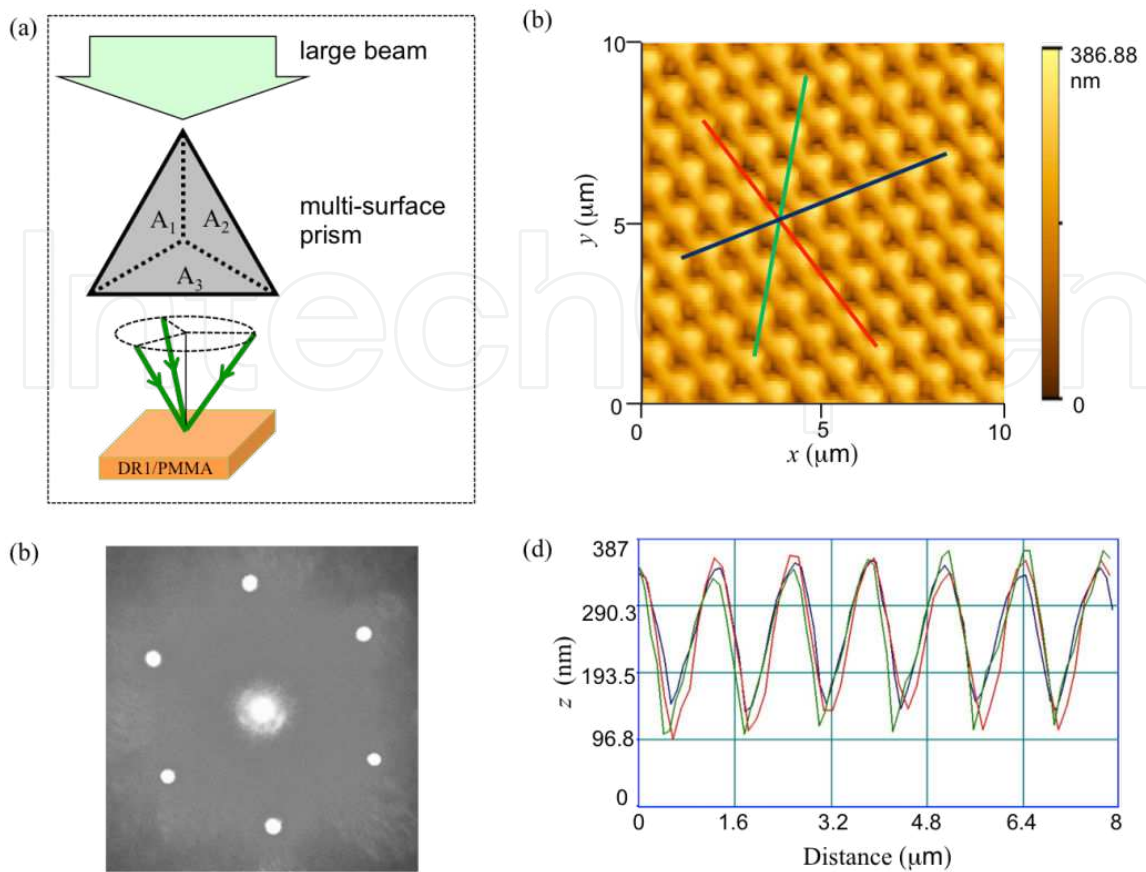


Figure 11. Realization of 2D periodic and symmetric SRG structure by one exposure to the three-beam interference pattern with C,C,C polarization configuration. (a) A large and uniform laser beam comes into a multi-surface prism and is divided into three sub-beams corresponding to surfaces denoted as A_1 , A_2 , and A_3 , respectively. The three beams overlap in an area in which a DR1/PMMA film is placed for the fabrication. (b) AFM image of a 2D SRG structure produced by three-beam interference with C,C,C polarization configuration. (c) Experimental diffraction pattern of the fabricated 2D SRG structure. (d) Surface modulation along three particular directions, as shown in figure (b), of the fabricated 2D SRG structure.

that, since the period belongs to the range for which the SRG depth is weak (see Fig. 7), the formation of the structure strongly depends on the relative ratio of the intensity of the three laser beams. A small difference of the intensities of the laser beams induces a deformation of the 2D SRG. Identical intensities of the three laser beams are therefore necessary for obtaining a perfect symmetry of the SRGs. The dependence of the symmetry of the 2D SRGs on the relative intensities and on different polarizations (S,S,S and P,P,P) of the laser beams is under investigation.

4. Optimization of SRG formation

Besides the realization of SRGs on azo-copolymer materials, it is also interesting to optimize the SRGs depth. Indeed, for a best choice of experimental parameters, the SRG amplitude is

obtained only about 30% of the thickness of the sample. Several methods have been proposed to improve the DE and the modulation depth of the SRGs, such as electrical poling, temperature effect, etc. [23-24]. In this work, we demonstrated a simple optical method, which allowed increasing rapidly the formation of the SRGs. This method is based on the control of the photoisomerization process between *trans*- and *cis*-forms of the DR1 molecules. We have demonstrated, as shown in the insert of the Fig. 1, that the use of an additional UV or VIS laser beam assists the *trans-cis-trans* cycle, resulting in a rapid rotation of the DR1 molecules. This optical assistance leads to the formation of SRGs with a large modulation depth. To understand the mechanism of this assisting effect, we describe the photoisomerization process of DR1 molecules (insert of Fig. 1) as follow: DR1 molecules undergo photoisomerization process from *trans*-form to *cis*-form by applying a green light. If we apply an assisting UV light beam simultaneously with the green beam, the *trans*-form becomes the *cis*-form (green excitation), and the *cis*-form rapidly returns to the *trans*-form (UV excitation). On the other hand, if we apply an assisting VIS light beam simultaneously with the green beam, the *trans*-form becomes the *cis*-form (green excitation), and the *cis*-form relaxes to the *trans*-form in the perpendicular direction, which is then transferred back to the *cis*-form thanks to the excitation of the assisting VIS beam. The *trans-cis-trans* cycle is therefore accelerated and multiplied, resulting in a SRG with larger amplitude.

Figure 12 (a) shows the optical arrangement of two interfering beams with an assisting beam. Two coherent green beams interfere and create SRG on DR1/PMMA sample. Another laser beam, whose wavelength is 355 nm (UV) or 532 nm (VIS), comes into the sample, at the interfering area to improve the formation of SRG. Here again, different polarization configurations of the writing and assisting beams are investigated, as shown in Fig.12 (b). All other parameters, such as the thickness of samples (about 1.7 μm), the writing time (long enough to reach the maximum SRG depth), the intensities of the writing beams and of the UV or VIS assisting beam, were kept unchanged.

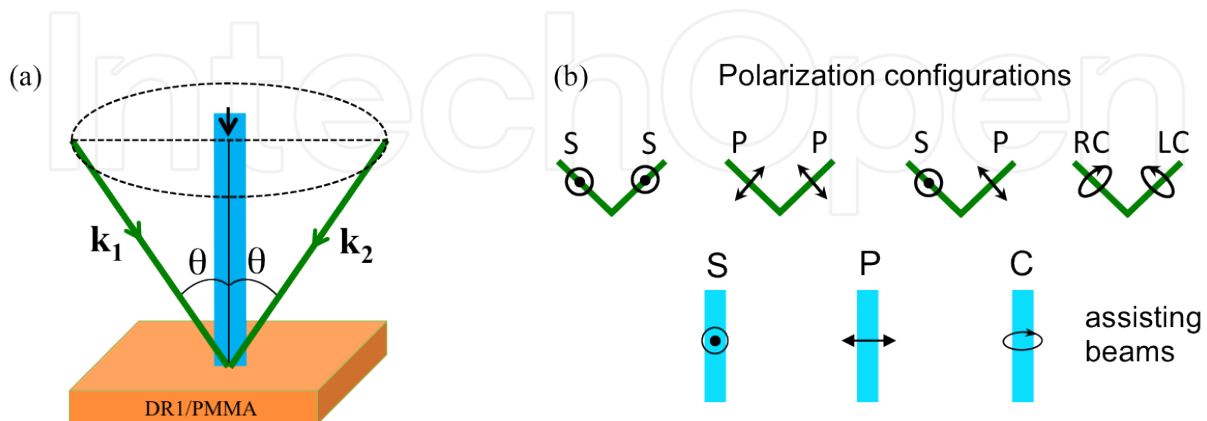


Figure 12. a) Optical arrangement of two-beam interference experiment with an additional assisting beam. Two green (VIS) beams interfere on the surface of the DR1/PMMA and an assisting beam comes into sample at normal incidence. (b) Different possibilities of polarization configurations of writing (VIS) and assisting beam (UV or VIS).

4.1. Assisting by UV beam

Figure 13 shows the intensity of the first-order diffraction and the modulation depth of the SRGs created with the assistance of the UV beam. We can observe clearly that the DE increases immediately and rapidly when the UV assisting beam is turned on (Figs. 13(a-c)) and reaches a maximum value, which is much higher than that obtained without the UV assisting beam. We also found that the assisting effect is polarization dependent, for both writing beams and assisting beams. The best polarization configuration for the improvement of SRG formation was identified, corresponding to the case in which the polarization of the UV assisting beam is same as the polarizations of the writing beam. The reason why such a polarization configuration is optimum could be found from the photoisomerization process. Indeed, the green beam transfers the *trans*-form to the *cis*-form, and the *cis*-form rapidly returns to the *trans*-form via the UV excitation. The polarization of the UV laser therefore should be as same as that of the green laser beam in order to act on the same molecule oriented in the same direction. Figures 13(d-f) show the SRG depths obtained in such an optimized polarization configuration. The SRG amplitude was improved from several nanometers to several hundred nanometers. The evolution of the SRG depth is similar to that of the DE, but is not exactly the same, in particular for the case of RC-LC writing beam polarization configuration.

4.2. Assisting by VIS beam

Another additional VIS beam, of the same wavelength as the writing beams (532 nm), was used instead of the UV beam to assist the formation of SRG. The DE also immediately increases and accordingly a SRG with large amplitude is obtained, similar to the results obtained from the UV assisting. Figure 14 shows the improvement of DE and the SRG depth for different polarization configurations. Considering only two particular polarizations, s- and p-polarizations, contrary to the case of UV assisting, the best improvement of SRG formation was obtained when the polarization of the VIS assisting beam is perpendicular to the polarizations of the writing beams. Here again, the mechanism of the VIS assisted SRG formation should be explained using the photoisomerization process. Indeed, when an assisting VIS light beam is simultaneously applied with the writing green beams, the *trans*-form is transferred to the *cis*-form (green excitation), the *cis*-form relaxes to the *trans*-form, which is oriented in perpendicular direction to the original *trans*-form (angular hole burning effect). The assisting VIS beam, whose polarization is perpendicular to those of the writing beams, therefore excites the new *trans*-form and enhances the photoisomerization process and consequently the SRG formation.

As compared with UV assisting, this VIS assisting technique is quite interesting for SRGs fabrication. Effectively, on one hand, a low cost VIS laser such as a green laser diode is sufficient to help the SRGs formation. On the other hand, a single green laser could be also split and delayed in time into two independent lasers sources, each one playing a role as writing and assisting beams, resulting in a simple and compact fabrication setup.

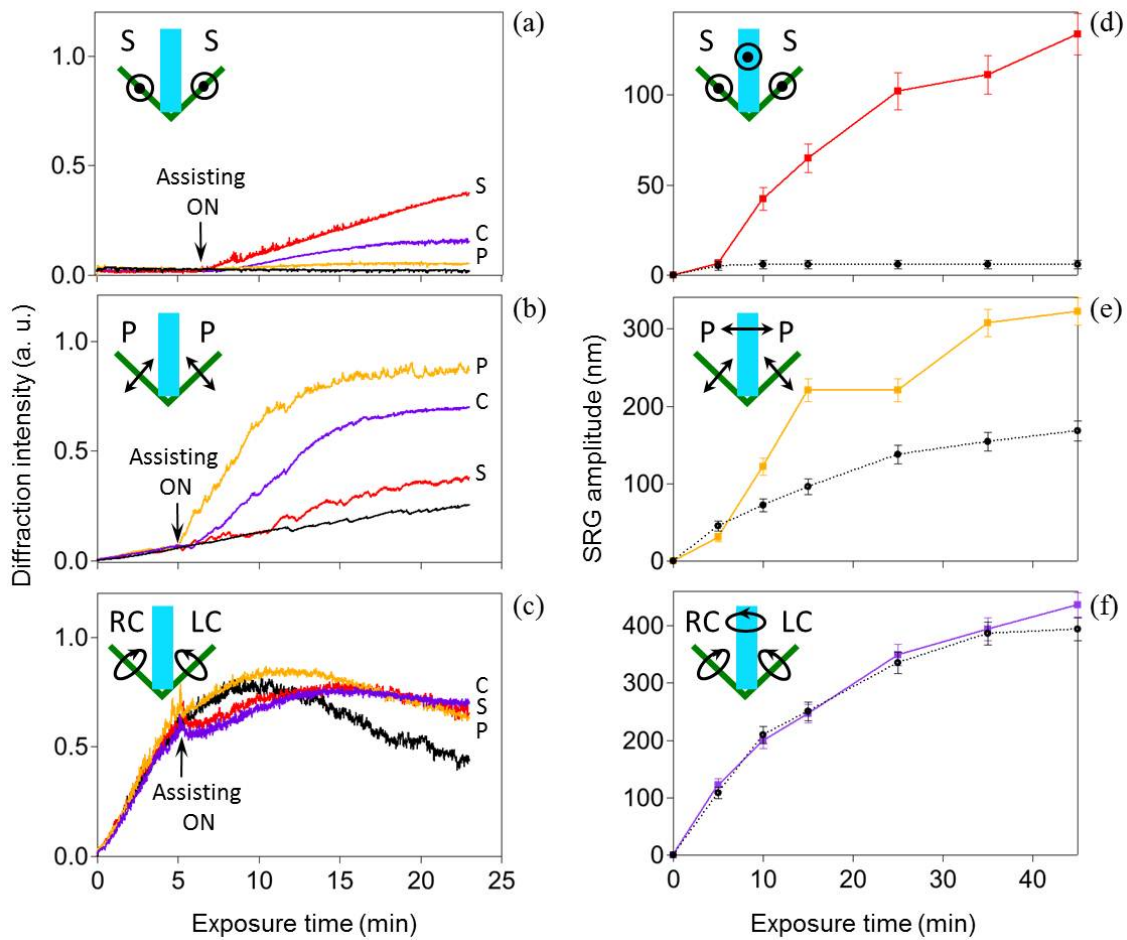


Figure 13. Optimization of SRG formation by an UV assisting beam. Left: time dependence of the first-order diffraction intensity. Right: improvement of the SRG depth as a function of time. The polarization configurations are illustrated in each figure. The black curves (left) and dots (right) show the results obtained without UV assisting beam, which are plotted in each figure in order to compare with those obtained with assisting beam.

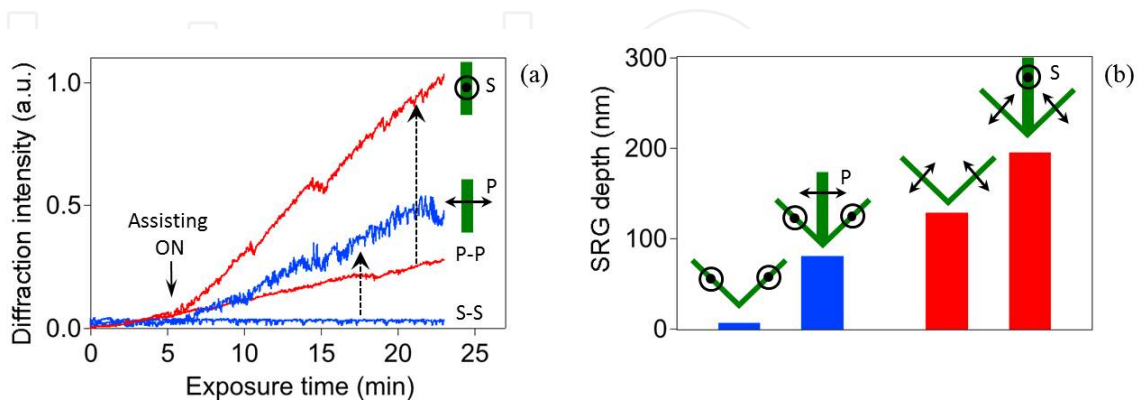


Figure 14. Optimization of SRG formation by a green incoherent beam. (a) Time dependence of the first-order diffraction intensity. (b) Comparison of the depth of the SRGs inscribed with and without green assisting beam for two particular polarization configurations, P-P (red) and S-S (blue).

5. Conclusion

The realization and optimization of 1D and 2D surface relief grating made of on azopolymer materials are in high demand for the use in many applications, such as holographic data storage, active waveguides, electro-optic modulators and also distributed-feedback lasers. In this chapter, simple fabrication techniques based on two-beam and three-beam interferences were theoretically and experimentally demonstrated as efficient methods for creation of desired SRGs on azo-copolymer. The interference patterns were theoretically analysed in detail for both intensity and polarization distributions. These two parameters are competitive and complementary for the formation of SRG. The polarization modulation is however experimentally demonstrated to be more important. Depending on the desired applications, 1D and 2D SRG could be fabricated by two-beam or three-beam interference, respectively. 2D SRGs with different configurations, e.g., hexagonal or square, have been fabricated by using a simple two-exposure of the two-beam interference pattern. The shape of the fabricated structures is however not symmetric due to the mechanism of the SRG formation. 2D hexagonal SRGs with perfect symmetry have been then fabricated by a single exposure of the three-beam interference pattern. We expect that a symmetric 2D square SRG could be also fabricated by using a four-beam interference pattern. Furthermore, it will be possible to fabricate quasi-periodic SRGs on demand by using a two-exposure of the three-beam interference or four-beam interference patterns.

Besides, two efficient optical methods were also proposed to enhance the formation of SRGs, employing an incoherent UV or VIS beam. These lasers assist the photoisomerization process of DR1 molecules, resulting in a rapid inscription and large amplitude of SRG. The polarization analysis has been experimentally investigated, showing different mechanisms of the two assisting laser beams. SRGs with largest amplitude were obtained when the polarizations of the writing beam and the UV beam are same and when the polarizations of the writing beam and the VIS beam are orthogonal. These properties help to understand the mechanism of the formation of SRG that is obviously not clear till now.

These periodic and quasi-periodic SRGs can be very useful for many photonic applications [25]. Application of 2D SRGs as nonlinear photonic crystals is under investigation. Fabrication of large-area 3D photonic crystals and nonlinear photonic crystals is also the objective of future work.

Acknowledgements

We would like to thank J. Lautru and A. Brosseau for invaluable help and access to the cleaning room and atomic force microscope. We also thank M. Dumont and Q. Li for useful discussion. This work was partially supported by Institute d'Alembert of the ENS Cachan. X. Wu acknowledges the fellowship from the China Scholarship Council, and T. T. N. Nguyen acknowledges the fellowship from the Vietnam International Education Development "322 program".

Author details

Xiao Wu^{1,2}, Thi Thanh Ngan Nguyen^{1,3}, Isabelle Ledoux-Rak¹, Chi Thanh Nguyen¹ and Ngoc Diep Lai^{1*}

*Address all correspondence to: nlai@lpqm.ens-cachan.fr

1 Laboratoire de Photonique Quantique et Moléculaire, UMR 8537 CNRS, Ecole Normale Supérieure de Cachan, France

2 Condensed Matter Physics, East China Normal University, Shanghai, China

3 Institute of Materials Sciences, Vietnam Academy of Science and Technology, Cau Giay, Hanoi, Vietnam

References

- [1] Goldenberg L. M., Lisinetskii V., Gritsai Y., Stumpe J., and Schrader S. Second Order DFB Lasing Using Reusable Grating Inscribed in Azobenzene-containing Material. *Optical Materials Express* 2012; 2 11-19.
- [2] Yariv A. Periodic Structures for Integrated Optics. *IEEE Journal of Quantum Electronics* 1977; 13 233-253.
- [3] Goldenberg L. M., Gritsai Y., Kulikovska O., and Stumpe J. Three-dimensional Planarized Diffraction Structures Based on Surface Relief Gratings in Azobenwene Materials. *Optics Letters* 2008; 33 1309-1311.
- [4] Viswanathan N. K., Kim D. Y., Bian S., Williams J., Liu W., Li L., Samuelson L., Kumar J., and Tripathy S. K. Surface Relief Grating on Azo Polymer Films. *Journal of Materials Chemistry* 1999; 9 1941-1955.
- [5] Natansohn A., and Rochon P. Photoinduced Motions in Azo-Containing Polymers. *Chemical Reviews* 2002; 102 4139-4175.
- [6] Pedersen T. G., Johansen P. M., Holme N. C. R., Ramanujam P. S., and Hvilsted S. Mean-Field Theory of Photoinduced Formation of Surface Reliefs in Side-chain Azobenzene Polymers. *Physical Review Letters* 1998; 80 89-92.
- [7] Kumar J., Li L., Jiang X. L., Kim D. Y., Lee T. S., and Tripathy S. K. Gradient Force: The Mechanism for Surface Relief Grating Formation in Azobenzene Functionalized Polymers. *Applied Physics Letters* 1998; 72 2096-2098.
- [8] Sumarua K., Yamanaka T., Fukuda T., and Matsuda H. Photoinduced Surface Relief Gratings on Azopolymer Films: Analysis by A Fluid Mechanics Model. *Applied Physics Letters* 1999; 75 1878-1880.

- [9] Fiorini C., Prudhomme N., Veyrac de G., Maurin I., Raimond P., and Nunzi J.-M. Molecular Migration Mechanism for Laser Induced Surface Relief Grating Formation. *Synthetic Metals* 2000; 115 121-125.
- [10] Baradaa D., Itoh M., and Yatagai T. Computer Simulation of Photoinduced Mass Transport on Azobenzene Polymer Films by Particle Method. *Journal of Applied Physics* 2004; 96 4204-4210.
- [11] Loucif-Saibi R., Nakatani K., Delaire J. A., Dumont M., and Sekkat Z. Photoisomerization and Second Harmonic Generation in Disperse Red One-doped and -functionalized Poly(methyl methacrylate) Films. *Chemistry of Materials* 1993; 5 229-236.
- [12] Sobolewska A., and Bartkiewicz S. Three Grating Coupling during the Holographic Grating Recording Process in Azobenzene-functionalized Polymer. *Applied Physics Letters* 2008; 92 253305(1-3).
- [13] Munakata K., Harada K., Itoh M., Umegaki S., and Yatagai T. A New Holographic Recording Material and Its Diffraction Efficiency Increase Effect: The Use of Photoinduced Surface Deformation in Azo-polymer Film. *Optics Communications* 2001; 191 15-19.
- [14] Bian S. P., Williams J. M., Kim D. Y., Li L., Balasubramanian S., Kumar J., and Tripathy S. Photoinduced Surface Deformations on Azobenzene Polymers Films. *Journal of Applied Physics* 1999; 86 4498-4508.
- [15] Kim D. Y., Li L., Jiang X. L., Shivshankar V., Kumar J., and Tripathy S. K. Polarized Laser Induced Holographic Surface Relief Grating on Polymer Films. *Macromolecules* 1995; 28 8835-8839.
- [16] Barrett C. J., Rochon P. L., and Natansohn A. L. Model of Laser-driven Mass Transport in Thin Films of Dye-Functionalized Polymers. *Journal of Chemical Physics* 1998; 109 1505-1516.
- [17] Barrett C. J., Natansohn A. L., and Rochon P. L. Mechanism of Optically Inscribed High-efficiency Diffraction Gratings in Azo Polymer Films. *Journal of Physics Chemistry* 1996; 100 8836-8842.
- [18] Lambeth R. H., Park J. Y., Liao H. W., Shir D. J., Jeon S. Rogers J. A., and Moore J. S. Proximity Field Nanopatterning of Azopolymer Thin Films. *Nanotechnology* 2010; 21 165301.
- [19] Lai N. D., Liang W. P., Lin J. H., Hsu C. C., and Lin. C. H. Fabrication of Two- and Three-dimensional Periodic Structures by Multi-exposure of Two-beam interference Technique. *Optics Express* 2005; 13 9605-9611.
- [20] Lai N. D., Liang W. P., Lin J. H., and Hsu C. C. Rapid Fabrication of Large-area Periodic Structures Containing Well-defined Defects by Combining Holography and Mask Techniques. *Optics Express* 2005; 13 1094-4087.

- [21] Lee S., Jeong Y. C., and Park J. K. Facile Fabrication of Close-packed Microlens Arrays Using Photoinduced Surface Relief Structures as Templates. *Optics Express* 2007; 15 14550-14559.
- [22] Berger V., Gauthier-Lafaye O., and Costard E. Photonic Band Gaps and Holography. *Journal of Applied Physics* 1997; 82 60-64.
- [23] Jager C., Bieringer T., and Zilker S. Bicolor Surface Reliefs in Azobenzene Side-chain Polymers. *Applied Optics* 2001; 40 1776-1778.
- [24] Yu H. F., Okano K., Shishido A., Ikeda T., Kamata K., Komura M., and Iyoda T. Enhancement of Surface-relief Gratings Recorded on Amphiphilic Liquid-crystalline Diblock Copolymer by Nanoscale Phase Separation. *Advanced Materials* 2005; 17 2184-2188.
- [25] Lee S., Kang H. S., and Park J. K. Directional Photofluidization Lithography: Micro/Nanostructural Evolution by Photofluidic Motions of Azobenzene Materials. *Advanced Materials* 2012; 24 2069-2103.